Supporting Information

Novel Metastable Hexagonal MoO_3 Nanobelts: Synthesis, Photochromic and Electrochromic Properties

*Lei Zheng, Yang Xu, Dong Jin, and Yi Xie**

Department of Nanomaterials and Nanochemistry, Hefei National Laboratory for Physical Sciences at Microscale, University of Science and Technology of China, Hefei, Anhui 230026, P. R. China

* To whom correspondence should be addressed. Fax: 86-551-3606266. E-mail: yxie@ustc.edu.cn

SI-1 TGA/DSC Curve of *h*-MoO_3 Nanobelts.

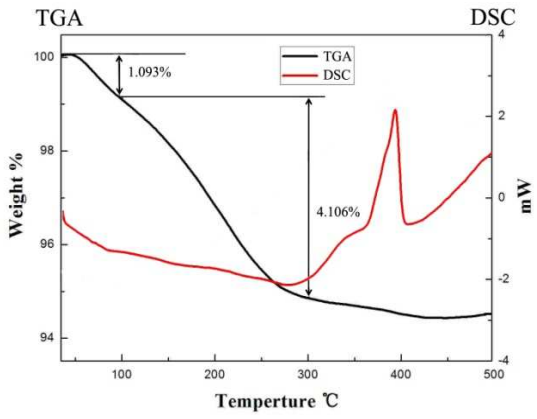

Figure S1. TGA/DSC curve of the *h*-MoO_3 nanobelts.

SI-2 Morphology of *h*-MoO_3 in Presence of Different Concentration $NaNO_3$.

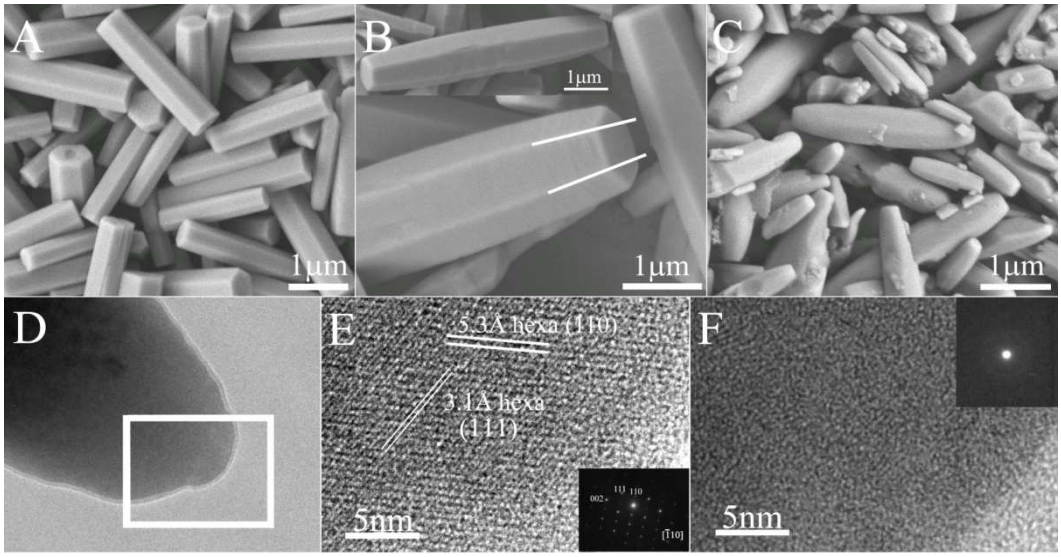

Figure S2. TEM images of the *h*-MoO_3 nanostructures fabricated at different amounts of $NaNO_3$: the amounts of $NaNO_3$ are (A) 1.0 g, (B) 1.5 g, and (C) 3.0 g. (D) The TEM image of a *h*-MoO_3 capsule-shaped microprism, showing a change from a crystalline (E) to amorphous (F) state under electron irradiation by HRTEM images and SAED patterns.

When 1.0 g $NaNO_3$ was used, the obtained products were all regular hexagonal microprisms in basal-faceted shape, as shown in **Fig. S2A**. Increasing the added amount of $NaNO_3$ to 1.5 g, it could be observed that the products tend to form capsule-shaped hexagonal microprisms with slightly curving arrises (in **Fig. S2B**). Once more $NaNO_3$ is introduced into the reaction system, significant change takes place in morphology and size of crystals. **Fig. S2C** shows the SEM images of the sample fabricated at 3.0g $NaNO_3$, which consists of capsule-shaped microprisms. The as-obtained sample is obviously small in size and nonuniform in shape. The corresponding HRTEM image and SAED of a unit plane (**Fig. S2D**) were shown in **Fig. S2E**. According to the HRTEM image, the prisms exhibit [-110] orientation, growing along the [001] direction. The clear lattice image and the sharp diffraction spots (inset) indicate the high crystallinity of the plane. Prolonging the electron

bombardment time to 5 min, all periodical lattices are also destroyed as the nanobelts, and the corresponding SAED pattern exhibits halo rings (as shown in **Fig. S2F**), indicating the instability of the hexagonal *h*-MoO_3 sample under strong electron beam.

SI-3 Experiments and Structural Characterization of Orthorhombic *α*-MoO_3 Nanobelts.

The orthorhombic *α*-MoO_3 nanobelts were easily obtained according to the reported route in Reference 13. In a typical procedure, molybdenum powders (2 mmol), deionized water (6 mL), and 30 wt% H_2O_2 aqueous solution (4 mL) were successively added into a Teflon vessel (15 mL) under magnetic agitation until metal powders were dissolved completely. Subsequently, the vessel was transferred into a stainless steel autoclave and hydrothermally treated at 150 °C for 12 h. After natural cooling, the white aqueous suspensions of *α*-MoO_3 nanobelts were obtained.

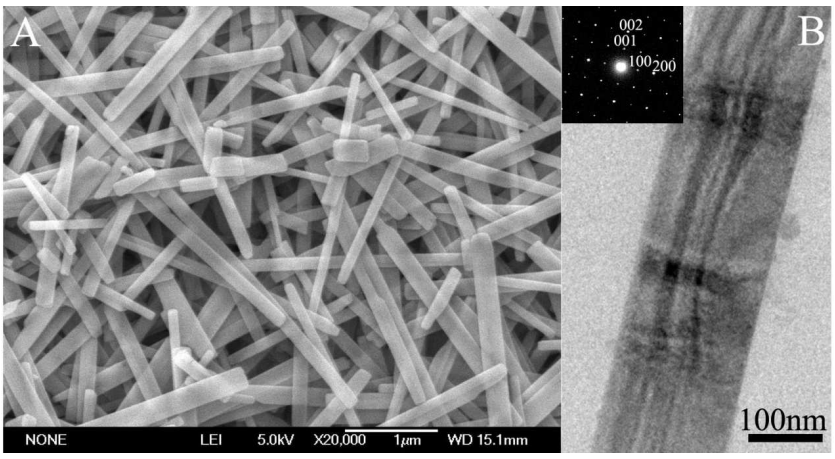

Figure S3. (A) TEM image of orthorhombic *α*-MoO_3 nanobelts. (b) TEM image of an individual *α*-MoO_3 nanobelt and its SAED pattern.

SI-4 Band Structures of *h*-MoO_3 and *α*-MoO_3 Calculated Based on Density Functional Theory Using the CASTEP Code Package.

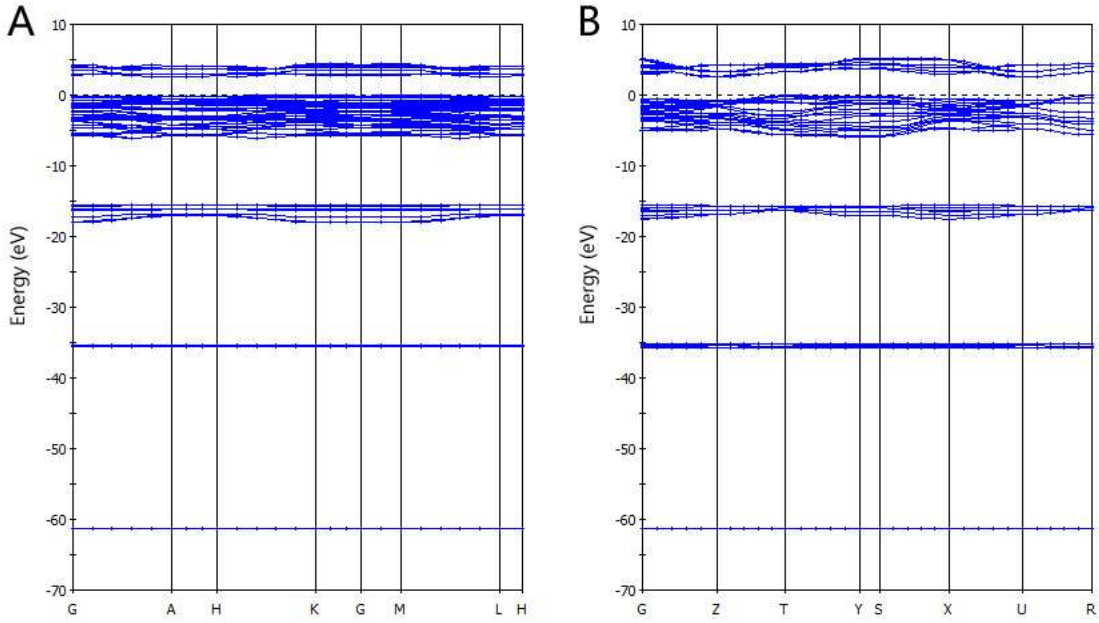

Figure S4. Calculated band structures of *h*-MoO_3 (A) and *α*-MoO_3 (B); the corresponding calculated bandgaps are 2.65 eV and 2.59 eV, respectively.

SI-5 Comparison of Photocatalytic Performance between *h*-MoO_3 and *α*-MoO_3.

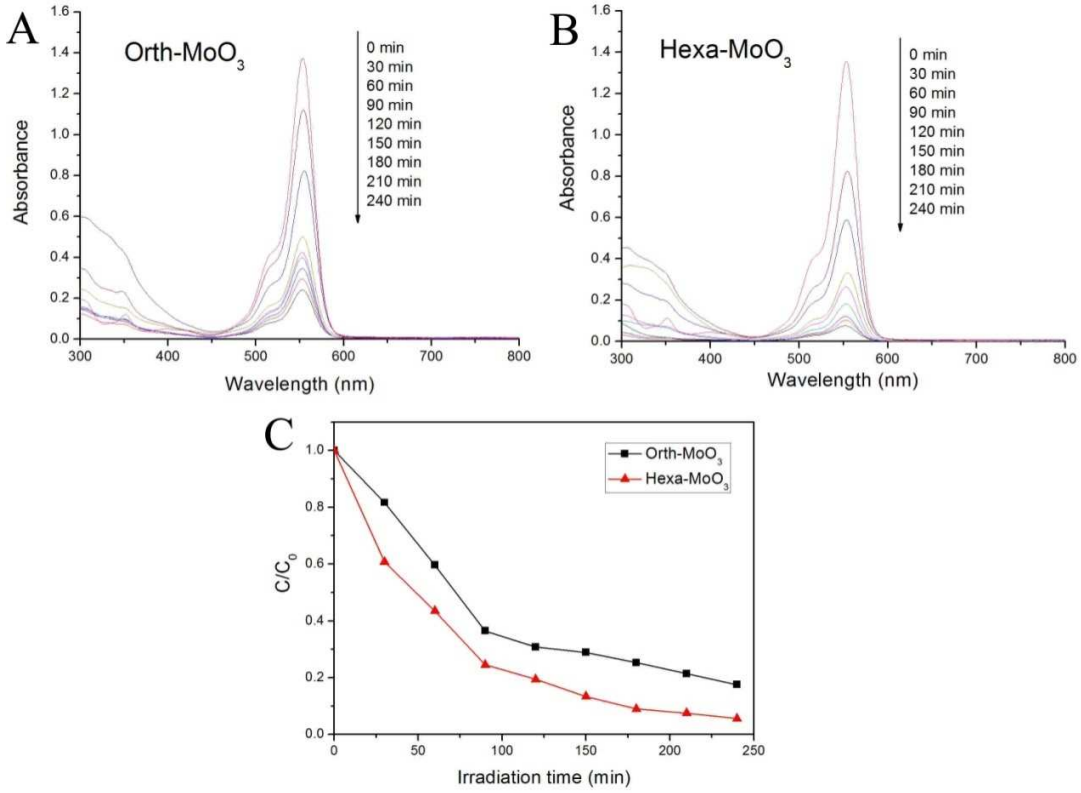

Figure S5. Comparative study on the photocatalytic performance for the degradation of Rhodamine B (RhB) with (A) orthorhombic *α*-MoO_3 nanobelts and (B) hexagonal *h*-MoO_3 nanobelts, and (C) a comparison of photocatalytic activities.

SI-6 Electrochromic performance of *h*-MoO_3 microprism sample.

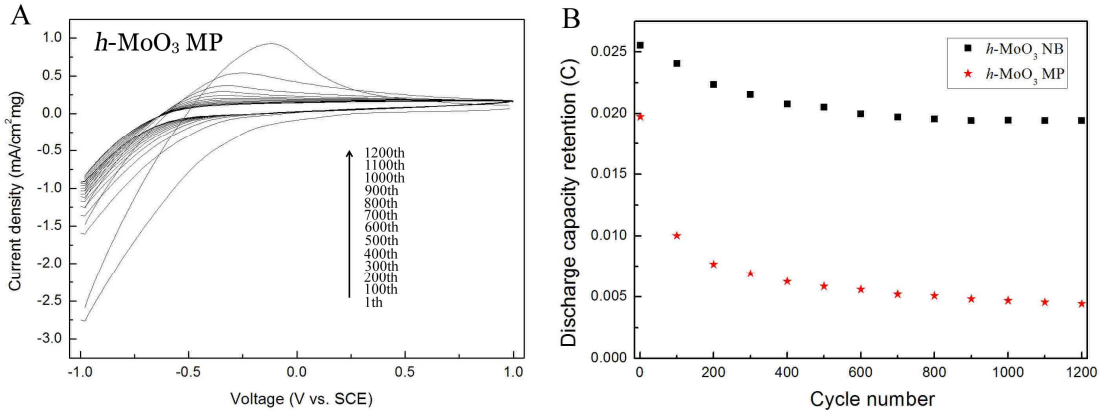

Figure S6. CV curves of the *h*-MoO_3 microprisms (MP) coated film for 1200th cycles, measured in 1.0 M $LiClO_4$/PC solution with a sweep rate of 0.1 V/s and discharge capacity retention comparison between the *h*-MoO_3 microprism and nanobelt samples coated film after different CV cycles.